Manganese-Induced Nephrotoxicity Is Mediated through Oxidative Stress and Mitochondrial Impairment

Amir Mohammad Niknahad[1,2], Mohammad Mehdi Ommati[3], Omid Farshad[1], Leila Moezi[1,2]*,
Reza Heidari[1]*

[1]Pharmaceutical Sciences Research Center, Shiraz University of Medical Sciences, Shiraz, Iran; [2]Department of Pharmacology, School of Medicine, Shiraz University of Medical Sciences, Shiraz, Iran; [3]College of Life Sciences, Shanxi Agricultural University, Taigu, Shanxi, Peoples' Republic of China

Abstract

Manganese (Mn) is an essential element that is incorporated in various metabolic pathways and enzyme structures. On the other hand, a range of adverse effects has been described in association with Mn overexposure. Mn is a well-known neurotoxic agent in mammals. Renal injury is another adverse effect associated with Mn intoxication. No precise mechanism for Mn nephrotoxicity has been identified so far. The current study was designed to evaluate the potential mechanisms of Mn-induced renal injury. Rats were treated with Mn (20 and 40 mg/mL, respectively, in drinking water) for 30 consecutive days. Markers of oxidative stress, as well as several mitochondrial indices, were assessed in the kidney tissue. Renal injury was evident in Mn-treated animals, as judged by a significant increase in serum BUN and creatinine. Moreover, urinalysis revealed a significant increase in urine glucose, phosphate, and protein in Mn-treated rats. Kidney histopathological alterations, including tubular atrophy, interstitial inflammation, and necrosis, were also detected in Mn-treated animals. Biomarkers of oxidative stress, including an increment in reactive oxygen species (ROS), lipid peroxidation, and oxidized glutathione (GSSG), were detected in Mn-treated groups. On the other hand, kidney glutathione (GSH) stores and total antioxidant capacity were depleted in Mn groups. Mn exposure was associated with significant mitochondrial depolarization, decreased mitochondrial dehydrogenases activity, mitochondrial permeabilization, and depletion of adenosine tri-phosphate (ATP) content. These data highlight oxidative stress and mitochondrial impairment as potential mechanisms involved in Mn-induced renal injury.

Keywords: energy crisis; manganism; mitochondria; renal failure; serum electrolyte waste

Introduction

Manganese (Mn) is a trace element incorporated in several metabolic pathways and in the structures of some vital enzymes (1, 2). However, it has also been found that Mn overexposure is associated with several deleterious adverse effects, such as neurotoxicity (1, 3–5). Renal injury and disturbances of serum electrolytes are the other adverse effects associated with Mn overexposure (6–8). There is no precise mechanism for Mn-induced nephrotoxicity.

The mechanism of Mn neurotoxicity is widely investigated (9). It has been found that Mn-induced oxidative stress

plays a central role in the adverse effects of this metal on the nervous system (9–12). It has been reported that Mn accumulates in cellular mitochondria through calcium (Ca^{2+}) channels (2). Hence, cellular mitochondria are critical targets for Mn cytotoxicity. Mitochondrial depolarization, mitochondria swelling, increased mitochondria-mediated reactive oxygen species (ROS) formation, and mitochondria-mediated cell death have been reported in different experimental models that investigated Mn neurotoxicity (9–13).

Renal tissue contains numerous mitochondria, the proper functioning of which guarantee appropriate energy (ATP) level required for the reabsorption process of chemicals (14–16). The mechanism of nephrotoxicity induced by several xenobiotics relies on mitochondrial impairment and mitochondria-mediated cell death (17). Oxidative stress and mitochondrial injury are two mechanistically related events (18). Hence, mitochondrial impairment could deteriorate oxidative stress and vice versa.

As already mentioned, there is no precise mechanism for Mn-induced renal injury. The current study was designed to evaluate the role of oxidative stress and mitochondrial impairment in the pathogenesis of Mn nephrotoxicity. Rats were exposed to Mn for 30 consecutive days. Several biomarkers in serum and urine, as well as histopathological alterations and oxidative stress markers in renal tissue, were evaluated. Moreover, kidney tissue mitochondria were isolated and assessed.

Materials and Methods

Reagents

3-[4,5dimethylthiazol-2-yl]-2,5-diphenyltetrazolium bromide (MTT), iodoacetic acid, potassium hydroxide, bovine serum albumin (BSA), methanol high performance liquid chromatography (HPLC) grade, 3-(N-morpholino) propane sulfonic acid (MOPS), 4,2Hydroxyethyl,1-piperazineethanesulfonic acid (HEPES), dimethyl sulfoxide (DMSO), thiobarbituric acid (TBA), glacial acetic acid, glutathione (GSH), malondialdehyde (MDA), 2′,7′ Dichlorofluorescein diacetate (DCFH-DA), acetonitrile HPLC grade, ethylene glycol-bis (2-aminoethyl ether)-N, N, N′, N′-tetraacetic acid (EGTA), sucrose, dithiothreitol (DTT), sodium chloride, and Rhodamine 123 were obtained from Sigma Chemical Co. (St. Louis, MO, USA). Manganese chloride ($MnCl_2$), trichloroacetic acid (TCA), and hydroxymethyl aminomethane hydrochloride (Tris-HCl) were purchased from Merck (Darmstadt, Germany).

Animals and treatments

Mature male Sprague–Dawley rats (200–250 g, live weight; n = 24) were obtained from Shiraz University of Medicine, Shiraz, Iran. Rats were maintained under standard conditions (22–24°C; 12:12 h, photo schedule; appropriate ventilation; and 40 ± 2% relative humidity). Animals had free access to tap water and a commercial rodents chow diet (RoyanFeed®, Isfahan, Iran). All procedures on experimental animals were performed in compliance with the ethical guidelines approved by the Shiraz University of Medical Sciences ethics committee (#95-01-36-11290). Animals were allotted to three groups (n = 8 in each group), and treated as follows: (i) Control (vehicle-treated); (ii) $MnCl_2$ (20 mg/mL in drinking water); and (iii) $MnCl_2$ (40 mg/mL in drinking water). Animals were treated for 42 consecutive days. On day 43, rats were anesthetized, and serum and kidney tissue samples were collected.

Sample collection

Animals were anesthetized (Thiopental 80 mg/kg, i.p). Blood was collected from the abdominal aorta and transferred to standard tubes (VACUSERA®, Serum gel, and clot activator tubes) for serum preparation. The kidney tissue was washed in ice-cooled (4°C) normal saline and used for further assessments. Kidney weight index (WI) was determined as WI = [wet weight of organ (g)/body weight (g)] × 100.

Reactive oxygen species

Renal tissue ROS levels were measured using dichlorofluorescein diacetate (DCFH-DA) as a fluorescent probe (19). Briefly, 10 μL of DCFH-DA (10 μM final concentration) was added to 990 μL of tissue homogenate (10% w: v in KCl buffer). Samples were incubated for 15 min at 37°C in the dark. Finally, the DCF fluorescence intensity was assessed using a fluorimeter (FLUOstar Omega®, BMG LABTECH, Germany; λ_{excit} = 485 nm and λ_{em} = 525 nm) (19).

Renal tissue lipid peroxidation

Thiobarbituric acid reactive substances (TBARS) in renal tissue were measured as an index of lipid peroxidation in the renal tissue (12, 20). Briefly, renal tissue (500 mg) was homogenized in ice-cooled KCl buffer (1.15% w: v; 4°C). Then, 500 μL of tissue homogenate was added to a reaction mixture consisting of 1 mL TBA (0.375%, w: v), 1 mL trichloroacetic acid (20% w: v), and meta-phosphoric acid (3 mL f 1% w: v solution, pH = 2) (21). The mixture was incubated in a water bath (100°C) for 45 min (22). Then, 4 mL of n-butanol was added and vortexed (1 min). Finally, samples were centrifuged (17,000 × g for 10 min) and the absorbance of the developed color in upper phase (n-butanol) was measured at λ = 532 nm (EPOCH® plate reader, Highland Park, USA) (21).

Renal tissue and mitochondria glutathione content

Renal glutathione levels (oxidized and reduced; GSSG and GSH) were measured by the HPLC method (23). The HPLC

system consisted of an NH_2 column as the stationary phase (25 cm, Bischoff chromatography, Leonberg, Germany) (24). The mobile phases consisted of buffer A (Water: Methanol; 1: 4 v: v) and buffer B (Acetate buffer: Buffer A; 1: 4 v: v), and a gradient method with a steady increase of buffer B to 95% in 25 min (24). The flow rate of the mentioned mobile phase was 1 mL/min, and the UV detector (UV) detector was set at $\lambda = 254$ nm. Tissue samples were homogenized in Tris-HCl buffer (250 mM; pH = 7.4; 4°C), and 500 μL of TCA (50% w: v) was added. Isolated mitochondria (1 mL, 1 mg protein/mL) were also treated with 100 μL of TCA 50% w: v. Samples were mixed well, incubated on ice (10 min), and centrifuged (17,000 g, 30 min, 4°C). Afterward, 1 mL of the supernatant was collected in 5 mL tubes and 300 μL of the NaOH: $NaHCO_3$ (2 M: 2 M) solution was added. Then, 100 μL of iodoacetic acid (1.5% w: v in deionized water) was added, and samples were incubated for 1 h (4°C, in the dark). Afterward, 2, 4-dinitrofluorobenzene (DNFB, 500 μL of 1.5% w: v in absolute ethanol) was added and mixed well. Samples were incubated in the dark (25°C, 24 h). Finally, samples were centrifuged (17,000 g, 30 min) and injected (25 μL) into the described HPLC system (23).

Protein carbonylation

The oxidative damage of kidney tissue proteins was assessed based on the reaction with dinitrophenyl hydrazine (DNPH) (25). Briefly, 1 mL of the tissue homogenate (10% w: v) was treated with 100 μL of the triton X-100 (0.1% w: v) and centrifuged (10 min, 700 g, 4°C). Then, 500 μL aliquots of the resulting supernatant were treated with 300 μL of DNPH (10 mM in HCl). Samples were then incubated for 1 h (25°C, vortexing every 10 min). Afterward, 100 μL of trichloroacetic acid (20% w: v) was added and centrifuged (12,000 g, 5 min) (26). The pellet was washed three times with ethanol: ethyl acetate (1 mL of 1: 1 v: v solution). Finally, the precipitate was re-dissolved in guanidine hydrochloride solution (600 μL of 6 M solution), and the absorbance at $\lambda = 370$ nm was measured (EPOCH® plate reader, Highland Park, USA) (25).

Ferric reducing antioxidant power

The ferric reducing antioxidant power (FRAP) of kidney tissue was measured (27). The FRAP assay measures change in the absorbance at $\lambda = 593$ nm due to the formation of a blue-colored ferrous (Fe^{2+})-4, 6-tripyridyl-s-triazine (TPTZ) complex from the colorless oxidized ferric form (Fe^{3+}) by the action of tissue electron-donating antioxidants. The working FRAP solution was freshly prepared by mixing 25 mL of acetate buffer (300 mmol/L; pH = 3.6) with 2.5 mL of TPTZ (10 mmol/L in 40 mmol/L HCl) and 2.5 mL of ferric chloride ($FeCl_2$, 20 mmol/L). Tissue samples (200 mg) were homogenized in 5 mL of 250 mM Tris-HCl buffer (pH = 7.4; 4°C). Afterward, 50 μL of tissue homogenate was added to 900 μL of the FRAP reagent and incubated in the dark (37°C, 5 min). The intensity of the resultant blue color was measured at $\lambda = 593$ nm using an EPOCH plate reader (BioTek® Instruments, Highland Park, US) (27).

Histopathological assessment

For histopathological evaluations, renal specimens were fixed in a buffered formalin solution prepared from NaH_2PO_4 (0.4% w: v), Na_2HPO_4 (0.64% w: v), and formaldehyde (10%) in double-distilled water (pH = 7.4). Paraffin-embedded tissue specimens were cut (5 μm) using a microtome and stained with hematoxylin and eosin. Kidney histopathological changes were evaluated using a light microscope (Olympus BX41; Olympus Optical Co. Ltd, Japan).

Renal and serum Mn levels

Serum and kidney Mn levels were measured using an inductively coupled plasma mass spectrometry (ICP-MS) method (28). Briefly, serum (500 μL) and kidney tissue samples (500 μL of 10% w: v tissue homogenate) were treated with 100 μL of nitric acid (HNO_3; 2.5% w: v) and centrifuged (17,000 g, 30 min). The supernatants were collected and used for Mn determination (28).

Kidney mitochondria isolation

Rats' kidneys were washed (NaCl 0.9% w: v, 4°C) and minced in the ice-cold isolation buffer containing 0.5 mM EGTA, 2 mM HEPES, 220 mM sucrose, 70 mM mannitol, and BSA (0.1% w: v) (pH = 7.4). Minced tissue was transported into fresh isolation buffer (5 mL buffer: 1 g tissue) and homogenized. Kidney mitochondria were isolated based on the differential centrifugation method (29). For this purpose, unbroken cells and nuclei were pelleted at the first round of centrifugation (1000 g for 10 min at 4°C). Afterward, the supernatant was centrifuged at 10,000 g (10 min at 4°C) to pellet the mitochondria fraction (brown-colored). The second centrifugation step was repeated at least thrice using a fresh buffer medium. Finally, mitochondrial pellets were resuspended in a buffer (5 mL buffer/g tissue) containing 70 mM mannitol, 220 mM sucrose, and 2 mM HEPES (pH = 7.4). The mitochondria fractions used to measure mitochondrial permeabilization and mitochondrial depolarization were suspended in mitochondria permeabilization buffer (65 mM KCl, 10 mM HEPES, 125 mM Sucrose, pH = 7.2) and depolarization assay buffer (220 mM Sucrose, 10 mM KCl, 68 mM Mannitol, 5 mM KH_2PO_4, 2 mM $MgCl_2$, 50 μM EGTA, and 10 mM HEPES, pH = 7.2) (29). Sample protein concentrations were determined based on the Bradford method to standardize the obtained data.

Mitochondrial dehydrogenases activity

A colorimetric technique based on the production of purple formazan crystals from the 3-(4, 5-dimethylthiazol-2-yl)-2, 5-diphenyltetrazolium bromide was used for the estimation of mitochondrial dehydrogenases activity (30). Briefly, a mitochondrial suspension (0.5 mg protein/mL) was incubated with 40 μL of MTT (0.4% w: v) and incubated in the dark (37°C, 30 min). Samples were centrifuged (15,000 g, 15 min), and the pellet was dissolved in dimethyl sulfoxide (DMSO; 1000 μL). The optical density (OD) at λ = 570 nm was measured with an EPOCH® plate reader (Highland Park, USA) (30).

Mitochondrial ATP levels

Based on a previously reported protocol, mitochondrial ATP level was assessed by HPLC (31, 32). Briefly, isolated mitochondria (1 mg protein/mL) were mixed with 100 μL ice-cooled meta-phosphoric acid solution (50% w: v, 4°C) and centrifuged (30 min, 17,000 *g*, 4°C). Afterward, the supernatant (100 μL) was treated with 15 μL of ice-cooled potassium hydroxide solution (KOH, 1 M). Samples were centrifuged (30 min, 17,000 *g*, 4°C) again, and 25 μL of the supernatant was injected into an HPLC system composed of an LC-18 column (μ-Bondapak, 25 cm). The mobile phase was composed of potassium hydrogen phosphate mono-basic (100 mM KH_2PO_4, pH = 7 adjusted with KOH), acetonitrile (2.5% v: v), and tetrabutylammonium hydroxide (1 mM). The flow rate was 1 mL/min, and the UV detector was set at λ = 254 nm (31).

Mitochondrial depolarization

Mitochondrial uptake of the cationic dye rhodamine 123 was applied for the evaluation of mitochondrial depolarization (33, 34). Rhodamine 123 accumulates in the mitochondrial matrix by facilitated diffusion. When the mitochondrion is depolarized, there is no facilitated diffusion, and the amount of rhodamine 123 in the supernatant will be increased (35). In the current investigation, the mitochondrial fractions (0.5 mg protein/mL; in the depolarization assay buffer) were incubated with 10 μM of rhodamine 123 (30 min, 37°C, in the dark). Afterward, samples were centrifuged (15,000 g, 10 min, 4°C) and the fluorescence intensity of the supernatant was monitored with a fluorimeter (FLUOstar Omega®; BMG, Germany; $λ_{excit}$ = 485 nm and $λ_{em}$ = 525 nm) (33, 36).

Mitochondrial permeabilization and swelling

Mitochondrial swelling was estimated by analyzing the changes in optical density at λ = 540 nm (34, 37). Briefly, isolated mitochondria (0.5 mg protein/ml) were suspended in the mitochondria permeabilization buffer (65 mM KCl, 125 mM Sucrose, 10 mM HEPES, pH = 7.2), and the absorbance was monitored (30°C, during 30 min of incubation) using an EPOCH® plate reader (Highland Park, USA). An increase in mitochondrial swelling is associated with a decrease in absorbance. The results are reported as maximal mitochondrial swelling amplitude (ΔOD 540 nm) (37).

Lipid peroxidation in kidney mitochondria

TBARS were measured in isolated kidney mitochondria. Previous studies mentioned that sucrose interferes with the lipid peroxidation test in isolated mitochondria preparations (37). Therefore, mitochondria preparations were washed once (to remove sucrose) in ice-cooled MOPS-KCl buffer (100 mM KCl, 50 mM MOPS, 4°C, pH = 7.4). For this purpose, isolated kidney mitochondria were suspended in 5 mL of MOPS-KCl buffer and centrifuged (15,000 g, 4°C, 20 min). The pellet was re-suspended in MOPS-KCl buffer and used for TBARs assay. The mitochondrial suspension (1 mg protein/mL) was mixed with 1 mL of a solution containing trichloroacetic acid (15% w: v), HCl (0.24 N), TBA (0.375% w: v), and Trolox (500 μM). Samples were heated for 15 min at 100°C (37). Then n-butanol (1 mL) was added and vortexed (5 min). Samples were centrifuged (15,000 *g*, 10 min), and the absorbance of the n-butanol phase (upper phase) was measured (EPOCH® plate reader, Highland Park, USA, λ = 532 nm) (37).

Statistical methods

Data are represented as mean ± SD. Data analysis was accomplished by the one-way analysis of variance (ANOVA) and the Tukey's multiple comparison test as the *post hoc* test. A $P < 0.05$ was considered as a statistically significant difference.

Results

Animal weight gain was significantly lower in the Mn-treated group (40 mg/mL) in comparison with control rats (Figure 1A). The kidney WI was also significantly lower in Mn 40 mg/mL group (Figure 1A). Serum and kidney tissue Mn levels were also significantly higher in Mn-treated animals (Figure 1B).

Significant deterioration in serum biochemical measurements indicates renal injury in Mn-treated rats (Table 1). Signs of hypophosphatemia were evident in the Mn group (Table 1). On the other hand, serum BUN and creatinine levels were significantly higher in Mn-exposed animals (20 and 40 mg/mL) (Table 1). Significant elevation in urine protein, alkaline phosphatase (ALP), γ-glutamyl transferase (γ-GT), and glucose level was also detected in Mn-treated rats (Table 2).
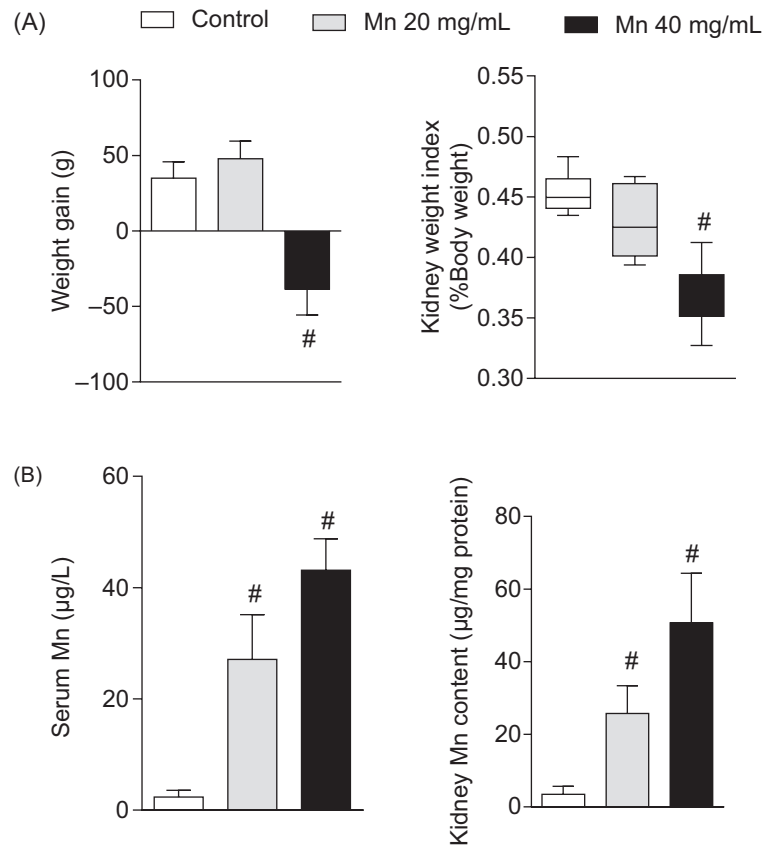
Figure 1. Effect of manganese treatment (20 and 40 mg/mL for 30 consecutive days) on animals' weight gain, renal weight index (Panel A), and serum and kidney tissue manganese (Mn) (Panel B).
Data are shown as mean ± SD (n = 8).
#Indicates significantly different as compared with the control group (P < 0.05).

Table 1. Serum biochemical measurements in manganese (Mn)-treated rats.

	Control	Mn 20 mg/mL	Mn 40 mg/mL
Ca^{2+} (mg/dL)	5.0 ± 0.20	4.9 ± 0.40	5.0 ± 0.50
K^+ (mmol/L)	5.5 ± 0.40	4.6 ± 0.32	4.5 ± 0.50
Na^+ (mmol/L)	84.0 ± 4.00	76 ± 3.00	71.0 ± 2.00
Glucose (mg/dL)	113.0 ± 9.00	105 ± 5.00	97.0 ± 11.00
Phosphate (mg/dL)	3.4 ± 0.40	2.33 ± 0.40	2.1 ± 0.11#
Total protein (mg/dL)	6.8 ± 0.44	7.1 ± 0.9	6.9 ± 0.30
Blood urea nitrogen (mg/dL)	43.0 ± 2.00	66.0 ± 5.00#	68 ± 4.00#
Creatinine (mg/dL)	0.3 ± 0.02	0.6 ± 0.03#	0.8 ± 0.03#

Data are represented as mean ± SD (n = 8).
#Indicates significantly different as compared with the control group (P < 0.01).

Table 2. Urinalysis of manganese (Mn)-treated animals.

	Control	Mn 20 mg/mL	Mn 40 mg/mL
Protein (mg/dL)	0.4 ± 0.1	1.1 ± 0.10#	1.2 ± 0.20#
ALP (U/L)	2122 ± 115	2380 ± 193	2670 ± 390#
γ-GT (U/L)	2569 ± 166	3134 ± 113	3897 ± 575#
Glucose (mg/dL)	80.0 ± 4.00	96.0 ± 19.00	132.0 ± 3.00#

Data are represented as mean ± SD (n = 8).
ALP: alkaline phosphatase; γ-GT: γ-glutamyl transferase.
#Indicates significantly different as compared with the control group (P < 0.01).
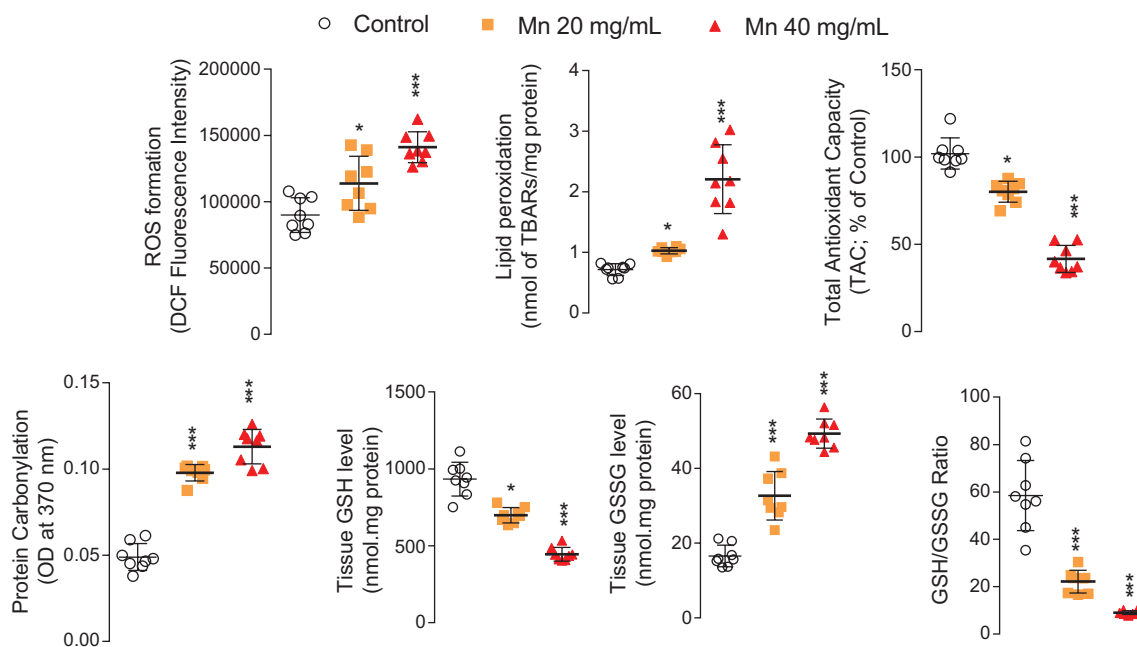
Figure 2. Markers of oxidative stress in the kidney tissue of manganese-treated rats.
Data are given as mean ± SD (n = 8).
Asterisks indicate significantly different from the control group (* P < 0.05, *** P < 0.001).

Significant ROS formation, lipid peroxidation, and protein carbonylation were detected in Mn groups (Figure 2). Moreover, kidney tissue GSH was depleted, and the GSSG level was significantly increased in Mn-exposed animals (Figure 2). Tissue antioxidant capacity was also dose-dependently decreased in the kidneys of Mn-treated rats (Figure 2).

Several mitochondrial indices were assessed in the kidney tissue of Mn-treated rats (Figure 3). It was found that Mn exposure significantly decreased mitochondrial dehydrogenases activity and ATP levels in a dose-dependent manner (Figure 3). Moreover, a significant increment of mitochondrial depolarization and swelling was detected in the kidney mitochondria of Mn-treated animals (Figure 3). Lipid peroxidation was also dose-dependently increased in the kidney mitochondria isolated from Mn-exposed animals (Figure 3).

Significant interstitial inflammation and tubular atrophy were evident in the kidneys of Mn 20 and 40 mg/mL groups (Figure 4 and Table 3). Moreover, Mn 40 mg/mL caused renal tissue necrosis (Figure 4 and Table 3).
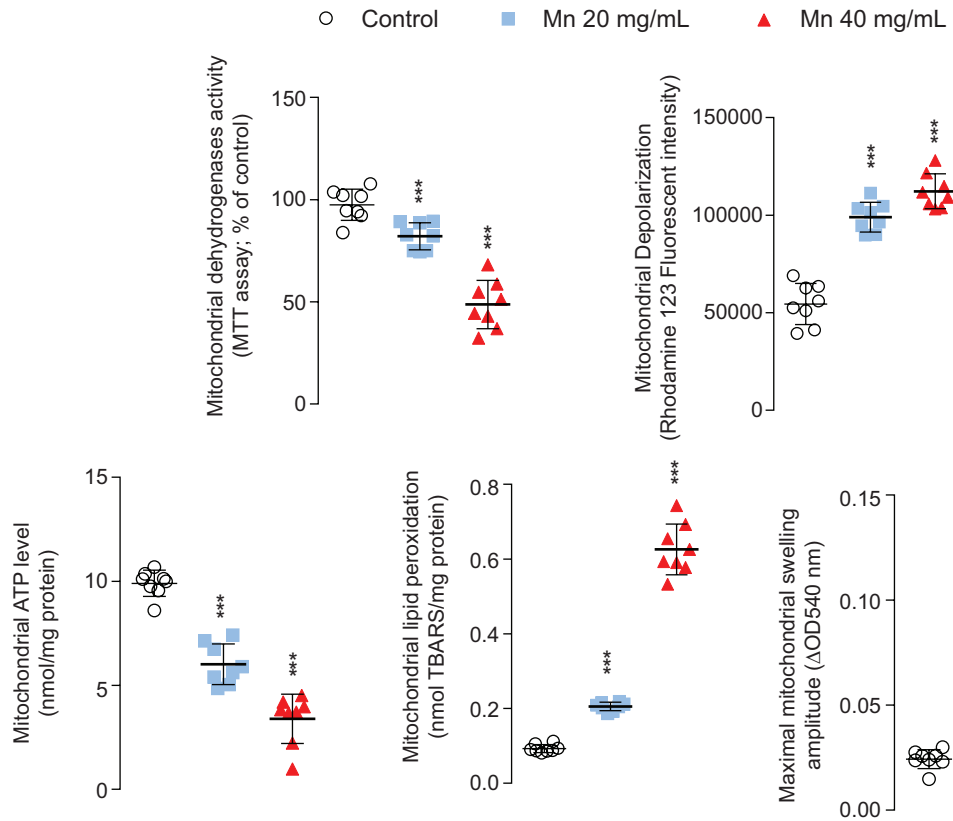
Figure 3. Markers of mitochondrial impairment in the kidneys of manganese-treated animals.
Data are presented as mean ± SD (n = 8).
*** Significantly different from the control group (P < 0.001).
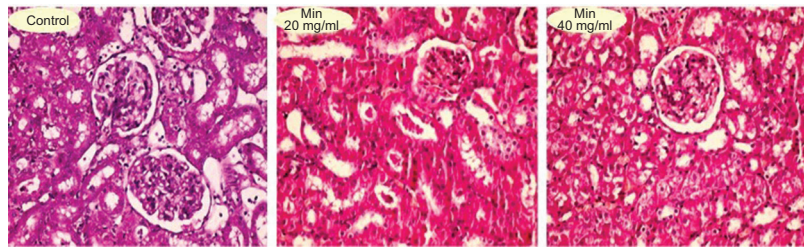
Figure 4. Kidney tissue histopathological alterations in manganese-exposed animals. Hematoxylin and eosin staining. The grades of histopathological changes are given in Table 3.

Table 3. Renal tissue histopathological alterations in manganese-exposed rats.

	Interstitial inflammation	**Tubular atrophy**	**Necrosis**
Control	−	−	−
Manganese 20 mg/mL	+	+	+
Manganese 40 mg/mL	++	++	+++

+: Mild; ++: Moderate; and +++: Severe histopathological alterations.

Discussion

Mn is a trace element that plays a fundamental role in several metabolic pathways and enzyme structures (2). However, overexposure to this metal is associated with a wide range of adverse effects, including renal injury (6–8, 38). Acute tubular necrosis, proteinuria, oliguria, and significant elevation in serum creatinine levels have been reported in human cases of Mn-induced nephrotoxicity (6, 38–40). No precise mechanism for Mn-induced nephrotoxicity has been identified so far. In the current investigation, it was found that Mn caused significant oxidative stress as well as mitochondrial impairment in the kidney tissue. The results might help in the development of therapeutic options against renal failure and serum electrolyte imbalance observed in Mn-intoxicated patients (6, 38–41).

Neurotoxicity is a well-described adverse effect of Mn (9, 13, 42–45). Oxidative stress and its consequences, such as disruption of biomembrane lipids and protein carbonylation, seem to play a fundamental role in Mn-induced toxicity in different organs such as the brain (9, 13, 42–45). Severe elevation in brain tissue ROS level and lipid peroxidation has been documented in Mn-induced neurotoxicity (9, 13, 42–45). Moreover, it has been found that brain tissue antioxidant systems are hampered upon Mn overexposure (9, 13, 42–45). The mechanism(s) of nephrotoxicity induced by Mn is less understood. Previous studies mentioned the occurrence of oxidative stress in the renal tissue of Mn-exposed animals (7). Mn-induced oxidative stress could affect several cellular targets, including biomembrane lipids, proteins, as well as deoxyribonucleic acid (7). In the current study, significant ROS formation, protein carbonylation, lipid peroxidation, and depletion of kidney tissue antioxidant capacity was evident in Mn-exposed rats. These results are consistent with previous investigations indicating Mn-induced oxidative stress in the kidney (7). Moreover, we found that kidney mitochondria could also be affected by Mn overexposure.

Cellular mitochondria are critical targets affected by Mn. (13). It has been found that Mn is accumulated in the mitochondrial matrix through Ca^{2+} channels (13). Induction of mitochondrial permeabilization, enhancement of mitochondria-facilitated ROS formation, a decrease of cellular ATP levels, and mitochondria-mediated cell death and apoptosis are associated with Mn-induced mitochondrial impairment (13).

Mitochondria play a fundamental role in kidney tissue (14–16). The reabsorption of chemicals (e.g., amino acids, glucose, and minerals) from nephrons to the bloodstream is an energy-dependent activity (14–16). Kidney tissue contains numerous mitochondria, the proper functioning of which guarantee enough ATP required for the reabsorption process of chemicals (14–16). Hence, Mn-induced mitochondrial impairment leads to an energy crisis and defect in the reabsorption of many chemicals in the renal tubules.

Consequently, serum electrolyte disturbances could occur. Cellular mitochondria are also important sites of ROS production (18). It has been repeatedly reported that xenobiotics-induced mitochondrial impairment could facilitate mitochondria-mediated ROS formation (18). Based on the data obtained from the current study, we might be able to speculate that Mn-induced mitotoxicity could serve as a major cause of oxidative stress in the renal tissue.

Conclusion

Collectively, our results indicate the fundamental role of oxidative stress and mitochondrial impairment in the pathogenesis of Mn-induced renal injury. Therefore, targeting cellular mitochondria might serve as a therapeutic point against Mn-induced nephrotoxicity.

Acknowledgments

Conflict of interest

The authors declare that there are no conflicts of interest.

References

1. Santamaria AB. Manganese exposure, essentiality & toxicity. Indian J Med Res. 2008;128(4):484–500.
2. Costa LG, Aschner M. Manganese in health and disease. London: Royal Society of Chemistry; 2014. 655 p.
3. Aschner M, Aschner JL. Manganese neurotoxicity: Cellular effects and blood-brain barrier transport. Neurosci Biobehav Rev. 1991;15(3):333–40. http://dx.doi.org/10.1016/S0149-7634(05)80026-0
4. Dobson AW, Erikson KM, Aschner M. Manganese neurotoxicity. Ann N Y Acad Sci. 2004;1012(1):115–28. http://dx.doi.org/10.1196/annals.1306.009
5. Pal PK, Samii A, Calne DB. Manganese neurotoxicity: A review of clinical features, imaging and pathology. Neurotoxicology. 1998;20(2–3):227–38.
6. Huang W-H, Lin J-L. Acute renal failure following ingestion of manganese-containing fertilizer. Clin Toxicol. 2004;42(3):305–7. http://dx.doi.org/10.1081/clt-120037433
7. Chtourou Y, Garoui EM, Boudawara T, Zeghal N. Protective role of silymarin against manganese-induced nephrotoxicity and oxidative stress in rat. Environ Toxicol. 2014;29(10):1147–54. http://dx.doi.org/10.1002/tox.21845
8. Sánchez-González C, López-Chaves C, Gómez-Aracena J, Galindo P, Aranda P, Llopis J. Association of plasma

manganese levels with chronic renal failure. J Trace Elem Med Biol. 2015;31:78–84. http://dx.doi.org/10.1016/j.jtemb.2015.04.001

9. Racette BA, Aschner M, Guilarte TR, Dydak U, Criswell SR, Zheng W. Pathophysiology of manganese-associated neurotoxicity. Neurotoxicology. 2012;33(4):881–6. http://dx.doi.org/10.1016/j.neuro.2011.12.010

10. Eftekhari A, Ahmadian E, Azarmi Y, Parvizpur A, Fard JK, Eghbal MA. The effects of cimetidine, N-acetylcysteine, and taurine on thioridazine metabolic activation and induction of oxidative stress in isolated rat hepatocytes. Pharm Chem J. 2018;51(11):965–9. http://dx.doi.org/10.1007/s11094-018-1724-6

11. Ommati MM, Heidari R, Ghanbarinejad V, Abdoli N, Niknahad H. Taurine treatment provides neuroprotection in a mouse model of manganism. Biol Trace Elem Res. 2018;190(2):384–95. http://dx.doi.org/10.1007/s12011-018-1552-2

12. Heidari R, Behnamrad S, Khodami Z, Ommati MM, Azarpira N, Vazin A. The nephroprotective properties of taurine in colistin-treated mice is mediated through the regulation of mitochondrial function and mitigation of oxidative stress. Biomed Pharmacother. 2019;109:103–11. http://dx.doi.org/10.1016/j.biopha.2018.10.093

13. Verity MA. Manganese neurotoxicity: A mechanistic hypothesis. Neurotoxicology. 1999;20(2–3):489–97.

14. Chakraborti S, Rahaman SM, Alam MN, Mandal A, Ghosh B, Dey K, Chakraborti T. Na+/K+-ATPase: A perspective. In: Chakraborti S, Dhalla NS, editors. Regulation of membrane Na+-K+ ATPase. Advances in biochemistry in health and disease. New York: Springer International Publishing; 2016. p. 3–30.

15. Bhargava P, Schnellmann RG. Mitochondrial energetics in the kidney. Nat Rev Nephrol. 2017;13(10):629–46. http://dx.doi.org/10.1038/nrneph.2017.107

16. Heidari R. The footprints of mitochondrial impairment and cellular energy crisis in the pathogenesis of xenobiotics-induced nephrotoxicity, serum electrolytes imbalance, and Fanconi's syndrome: A comprehensive review. Toxicology. 2019;423:1–31. http://dx.doi.org/10.1016/j.tox.2019.05.002

17. Ralto KM, Parikh SM, editors. Mitochondria in acute kidney injury. Semin Nephrol. 2016;36(1):8–16. http://dx.doi.org/10.1016/j.semnephrol.2016.01.005

18. Brookes PS, Yoon Y, Robotham JL, Anders MW, Sheu S-S. Calcium, ATP, and ROS: A mitochondrial love-hate triangle. Am J Physiol. 2004;287(4):C817–33. http://dx.doi.org/10.1152/ajpcell.00139.2004

19. Heidari R, Ghanbarinejad V, Mohammadi H, Ahmadi A, Esfandiari A, Azarpira N, et al. Dithiothreitol supplementation mitigates hepatic and renal injury in bile duct ligated mice: Potential application in the treatment of cholestasis-associated complications. Biomed Pharmacother. 2018;99:1022–32. http://dx.doi.org/10.1016/j.biopha.2018.01.018

20. Ommati MM, Heidari R, Zamiri MJ, Sabouri S, Zaker L, Farshad O, et al. The footprints of oxidative stress and mitochondrial impairment in arsenic trioxide-induced testosterone release suppression in pubertal and mature F1-male Balb/c mice via the downregulation of 3β-HSD, 17β-HSD, and CYP11a expression. Biol Trace Elem Res. 2020;95(1):125–34. http://dx.doi.org/10.1007/s12011-019-01815-2

21. Heidari R, Ghanbarinejad V, Mohammadi H, Ahmadi A, Ommati MM, Abdoli N, et al. Mitochondria protection as a mechanism underlying the hepatoprotective effects of glycine in cholestatic mice. Biomed Pharmacother. 2018;97(Supplement C):1086–95. http://dx.doi.org/10.1016/j.biopha.2017.10.166

22. Jamshidzadeh A, Heidari R, Latifpour Z, Ommati MM, Abdoli N, Mousavi S, et al. Carnosine ameliorates liver fibrosis and hyperammonemia in cirrhotic rats. Clin Res Hepatol Gastroenterol. 2017;41(4):424–34. http://dx.doi.org/10.1016/j.clinre.2016.12.010

23. Truong DH, Eghbal MA, Hindmarsh W, Roth SH, O'Brien PJ. Molecular mechanisms of hydrogen sulfide toxicity. Drug Metab Rev. 2006;38(4):733–44. http://dx.doi.org/10.1080/03602530600959607

24. Heidari R, Mandegani L, Ghanbarinejad V, Siavashpour A, Ommati MM, Azarpira N, et al. Mitochondrial dysfunction as a mechanism involved in the pathogenesis of cirrhosis-associated cholemic nephropathy. Biomed Pharmacother. 2019;109:271–80. http://dx.doi.org/10.1016/j.biopha.2018.10.104

25. Levine RL, Garland D, Oliver CN, Amici A, Climent I, Lenz A-G, et al. Determination of carbonyl content in oxidatively modified proteins. Methods Enzymol. 1990;186:464–78. http://dx.doi.org/10.1016/0076-6879(90)86141-h

26. Jamshidzadeh A, Heidari R, Mohammadi-Samani S, Azarpira N, Najbi A, Jahani P, et al. A comparison between the nephrotoxic profile of gentamicin and gentamicin nanoparticles in mice. J Biochem Mol Toxicol. 2015;29(2):57–62. http://dx.doi.org/10.1002/jbt.21667

27. Ommati M, Heidari R, Manthari R, Tikka SCJ, Niu R, Sun Z, et al. Paternal exposure to arsenic resulted in oxidative stress, autophagy, and mitochondrial impairments in the HPG axis of pubertal male offspring. Chemosphere. 2019;236:124325. http://dx.doi.org/10.1016/j.chemosphere.2019.07.056

28. Kihira T, Mukoyama M, Ando K, Yase Y, Yasui M. Determination of manganese concentrations in the spinal cords from amyotrophic lateral sclerosis patients by inductively coupled plasma emission spectroscopy. J Neurol Sci. 1990;98(2):251–8. http://dx.doi.org/10.1016/0022-510X(90)90266-P

29. Fernández-Vizarra E, Ferrín G, Pérez-Martos A, Fernández-Silva P, Zeviani M, Enríquez JA. Isolation of mitochondria for biogenetical studies: An update. Mitochondrion. 2010;10(3):253–62. http://dx.doi.org/10.1016/j.mito.2009.12.148

30. Ommati MM, Jamshidzadeh A, Heidari R, Sun Z, Zamiri MJ, Khodaei F, et al. Carnosine and histidine supplementation blunt lead-induced reproductive toxicity through antioxidative and mitochondria-dependent mechanisms. Biol Trace Elem Res. 2018;187:151–62. http://dx.doi.org/10.1007/s12011-018-1358-2

31. Chen Y, Xing D, Wang W, Ding Y, Du L. Development of an ion–pair HPLC method for investigation of energy charge changes in cerebral ischemia of mice and hypoxia of Neuro-2a cell line. Biomed Chromatogr. 2007;21(6):628–34. http://dx.doi.org/10.1002/bmc.798

32. Heidari R, Jafari F, Khodaei F, Shirazi Yeganeh B, Niknahad H. Mechanism of valproic acid-induced Fanconi syndrome involves mitochondrial dysfunction and oxidative stress in rat kidney. Nephrology. 2018;23(4):351–61. http://dx.doi.org/10.1111/nep.13012

33. Ahmadian E, Babaei H, Mohajjel Nayebi A, Eftekhari A, Eghbal MA. Mechanistic approach for toxic effects of bupropion in primary rat hepatocytes. Drug Res. 2017;67(4):217–22. http://dx.doi.org/10.1055/s-0042-123034

34. Heidari R, Niknahad H. The role and study of mitochondrial impairment and oxidative stress in cholestasis. In: Vinken M, editor. Experimental cholestasis research. Methods in molecular biology. New York, NY: Springer; 2019. p. 117–32.

35. Ommati MM, Heidari R, Jamshidzadeh A, Zamiri MJ, Sun Z, Sabouri S, et al. Dual effects of sulfasalazine on rat sperm

characteristics, spermatogenesis, and steroidogenesis in two experimental models. Toxicol Lett. 2018;284:46–55. http://dx.doi.org/10.1016/j.toxlet.2017.11.034

36. Heidari R, Niknahad H, Sadeghi A, Mohammadi H, Ghanbarinejad V, Ommati MM, et al. Betaine treatment protects liver through regulating mitochondrial function and counteracting oxidative stress in acute and chronic animal models of hepatic injury. Biomed Pharmacother. 2018;103:75–86. http://dx.doi.org/10.1016/j.biopha.2018.04.010

37. Caro AA, Adlong LW, Crocker SJ, Gardner MW, Luikart EF, Gron LU. Effect of garlic-derived organosulfur compounds on mitochondrial function and integrity in isolated mouse liver mitochondria. Toxicol Lett. 2012;214(2):166–74. http://dx.doi.org/10.1016/j.toxlet.2012.08.017

38. Sánchez B, Casalots-Casado J, Quintana S, Arroyo A, Martín-Fumadó C, Galtés I. Fatal manganese intoxication due to an error in the elaboration of Epsom salts for a liver cleansing diet. Forensic Sci Int. 2012;223(1–3):e1–4. http://dx.doi.org/10.1016/j.forsciint.2012.07.010

39. Young RJ, Critchley JA, Young KK, Freebairn RC, Reynolds AP, Lolin YI. Fatal acute hepatorenal failure following potassium permanganate ingestion. Hum Exp Toxicol. 1996;15(3):259–61. http://dx.doi.org/10.1177/096032719601500313

40. Agrawal VK, Bansal A, Kumar R, Kumawat BL, Mahajan P. Potassium permanganate toxicity: A rare case with difficult airway management and hepatic damage. Indian J Crit Care Med. 2014;18(12):819–21. http://dx.doi.org/10.4103/0972-5229.146318

41. Taylor PA, Price JD. Acute manganese intoxication and pancreatitis in a patient treated with a contaminated dialysate. Can Med Assoc J. 1982;126(5):503–5.

42. Erikson KM, Aschner M. Manganese neurotoxicity and glutamate-GABA interaction. Neurochem Int. 2003;43(4–5):475–80. http://dx.doi.org/10.1016/S0197-0186(03)00037-8

43. Erikson KM, Dobson AW, Dorman DC, Aschner M. Manganese exposure and induced oxidative stress in the rat brain. Sci Total Environ. 2004;334–335:409–16. http://dx.doi.org/10.1016/j.scitotenv.2004.04.044

44. Zwingmann C, Leibfritz D, Hazell AS. Brain energy metabolism in a sub-acute rat model of manganese neurotoxicity: An ex vivo nuclear magnetic resonance study using [1-13C]glucose. Neurotoxicology. 2004;25(4):573–87. http://dx.doi.org/10.1016/j.neuro.2003.08.002

45. Sarkar S, Malovic E, Harischandra DS, Ngwa HA, Ghosh A, Hogan C, et al. Manganese exposure induces neuroinflammation by impairing mitochondrial dynamics in astrocytes. Neurotoxicology. 2018;64:204–18. http://dx.doi.org/10.1016/j.neuro.2017.05.009